Computational Fluid Dynamics aided investigation and optimization of a tunnel-ventilated poultry house in China

Longhuan Du*, Chaowu Yang#, Robert Dominyξ, Li Yang#, Chenming Hu#, Huarui Du#, Qingyun Li#, Chunlin Yu#, Lingzhi Xie *, Xiaosong Jiang#,1

* School of Architecture and Environment, Sichuan University, Chengdu, China.

\# Animal Breeding and Genetics Key Laboratory of Sichuan Province, Sichuan Animal Science Academy, Chengdu, China.

ξ Faculty of Engineering and Environment, Department of Mechanical & Construction Engineering, Northumbria University, Newcastle, UK.

[1]Corresponding author: Xiaosong Jiang

Address: Sichuan Animal Science Academy, No.7, Niusha Road, Jinjiang District, Chengdu, Sichuan Province, 610066, China.

E-mail: xsjiang2017@163.com

Tel: 0086-28-84545177

℃

ABSTRACT

Ventilation system is crucial for poultry houses to control the indoor climate and air quality. The tunnel ventilation system is widely applied for large-scale poultry buildings in China but only limited scientific researches regarding the flow pattern, temperature distribution and design criteria are available in the literature. Thanks to the fast development of computer technology, Computational Fluid Dynamics (CFD) techniques were used in present study to investigate the indoor air movement, air temperature and relatively humidity. A three-dimensional CFD model was built according to the real dimensions of a laying hen house and the model was validated by comparing the simulation results with the field measurements at 30 positions. Meanwhile, statistical analysis was performed to determine the differences between different boundary conditions regarding the agreement between measured and CFD simulated results. Optimization of air inlet configurations was performed by using the validated CFD model and it was found that the uniformity of indoor air movement could prevent excessive local convective heat losses and reduce the temperature at the end of the house. Furthermore, the air inlets placed at the middle of the side wall could significantly reduce the high temperature expected at the end of the building without using extra energy, which is especially important for large-scale poultry farms with long buildings. The performance of side-wall windows was also examined and preliminary guidance was provided to effectively regulate the indoor climate by using these windows with the help of environmental monitoring systems. The present study contributes to the understanding and design of the tunnel ventilation system used in poultry houses.

Key words: poultry house, tunnel ventilation, indoor environmental parameters, uniform flow, design optimization

1 INTRODUCTION

The indoor environment of poultry houses plays a decisive role in the ultimate success of a poultry farm. Air temperature, relative humidity, air movement and air quality directly affect the thermal comfort and homeostasis of the birds. When the outdoor climate is hot and humid, the efficiency of evaporative cooling systems decreases significantly (Blanes-Vidal et al., 2008). Consequently, the indoor air temperature and relative humidity (RH) could rise above recommended levels due to the heat generated by the birds and bio-degradation (Blanes-Vidal et al., 2008; Oloyo, 2018). Therefore, under these circumstances the air velocity and movement play a crucial role in convectional cooling and regulation of air quality. Poultry farms with inadequate ventilation systems or non-uniform indoor air velocity distribution would suffer high mortality rates (Blanes-Vidal et al., 2008). So the ventilation systems of poultry houses should be carefully designed in order to ensure a comfort indoor climate for the birds.

China is one of the largest poultry-related products manufacturing and consuming countries in the world. Nowadays, for the majority of large-scale poultry buildings in China, the indoor air is conditioned for most of the year by means of climate control systems that consist of automatically regulated mechanical ventilation, radiator and evaporative cooling equipment. With regard to the type of the ventilation, the most widely used type in China for both broiler and laying hen houses is tunnel ventilation system although other types of ventilation such as cross ventilation and single-sided ventilation are popular in USA and European countries (Blanes-Vidal et al., 2008; Calvet et al., 2010; Bustamante et al., 2013; Bustamante et al., 2015; Bustamante et al., 2017).

One of the most widely adopted tunnel ventilation strategies in China is to apply the side wall inlets with the evaporation cooling pad installed behind the inlets. The outlet fans were placed at the end of the house and the air is drawn into one end of the house and exhausted at the other end. To avoid cold air supply directly into caged-hen occupied zone, bottom hinged flaps are installed to direct the cold incoming air to the upper part of house and mix with warm air there before entry into occupied zone (Cheng et al., 2018a). Although the tunnel ventilation is widely applied, limited studies (Xin et al., 1994; Wheeler et al., 2003; Cheng et al., 2018a; Tong et al., 2018) were performed to standardize and optimize its design and operation in the literature. Therefore, the use of scientific methods to study and optimize the effectiveness of this ventilation system is essential.

The current designs of standard poultry houses including the ventilation systems are usually evaluated by using direct measurement tools (Lee et al., 2003; Wheeler et al., 2003). However, direct measurement of the indoor environmental parameters (e.g. air velocity and temperature) has five main drawbacks: (1) the prerequisite of the field measurement is the existence of a building; (2) the number of points that can be measured is limited, making it difficult to obtain a comprehensive understanding of the indoor flow pattern or temperature distribution; (3) it is difficult to get a knowledge of the dynamic change of all environmental parameters by using the direct measurement tools; (4) the tools used to perform the direct measurement would unavoidably interfere with the air velocity and distort the measurements to some extent (Blanes-Vidal et al., 2008); (5) the field measurements are time-consuming and high cost. As a result, the number of field measurement related studies in the literature is limited and such studies generally cannot provide universal conclusions.

In recently years, the Computational Fluid Dynamics (CFD) technique has been widely used in studying ventilation systems of livestock buildings especially in USA and Northern Europe (Bjerg et al., 2002; Norton et al., 2009; Norton et al., 2010; Bjerg et al., 2013; Rahman et al., 2014; Rong et al., 2014; Rong et al., 2015). Once a CFD model is built, different types of studies can be performed. For example, various studies have analyzed the indoor flow pattern (Sun et al., 2002), the influence of sub-model representing heat and mass sources from animals and litter (Rojano et al., 2014; Rojano et al., 2015), and the impact of different boundary conditions on the internal field velocity(Lee et al., 2007; Blanes-Vidal et al., 2008). There are a few papers referring to the application of CFD models in studying naturally single-sided ventilation, cross-mechanical ventilation, tunnel ventilation and mechanical single-sided ventilation for poultry houses (Allocca et al., 2003; Blanes-Vidal et al., 2008; Salvet et al., 2010; Bustamante et al., 2013; Zajicek and Kic, 2013; Bustamante et al., 2015; Rojano et al., 2016; Bustamante et al., 2017; Cheng et al., 2018). However, it is noted that CFD technique has not been widely applied to study the tunnel ventilation system used in poultry houses.

Therefore, the overall aim of present study is to make contributions to the evaluation of indoor environmental parameters for tunnel-ventilated poultry houses. The objectives of this work are:

- Develop a three-dimensional CFD model with different boundary conditions to simulate the indoor airflow, air temperature and relative humidity distribution.
- Validate the CFD model by comparing simulated results with the field measurements from an experimental-oriented tunnel-ventilated laying hen house.

- Provide scientific data to evaluate the performance of the ventilation system and provide guidance to optimize the ventilation design by using the validated CFD model.

2. MATERIALS AND METHODS

2.1 Experiments

2.1.1 Experimental building

The experimental measurements were performed in a experimental-oriented laying hen house, equipped with tunnel ventilation system and located in Chengdu city, Sichuan Province, China (30.47 N, 103.73 E), as shown in Figure 1. It was a small-scale poultry house which had walls and suspended ceiling made of polystyrene serving as an insulator. The dimensions of the building were length, 40 m, width, 9.2 m, height (suspended ceiling height), 2.5 m. This laying hen house was provided with 2 side-wall air inlets (or referred as tunnel inlets) located at the front end of the house and the dimensions of the side-wall air inlets are illustrated in Figure 2a. 3 fans were installed at the end wall of the house each with a diameter of 1.27 m and there were in total 32 side-wall windows (see Figure 1b), each 56 cm wide and 27 cm high as shown in Figure 2b. For the 2 air inlets and all side-wall windows, a bottom hinged flap mechanism was used to control the opening angle, enabling a control range from 0° (fully closed) to 90° (fully open).

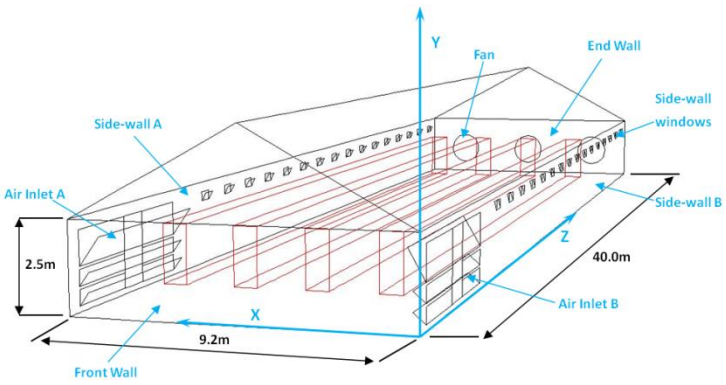

(a) (b)

Figure 1. (a) Photograph of the side view of the laying hen house, (b) schematic drawing of the house (the red rectangular cuboids indicate the simplified animal occupied zone) and the origin of coordinate used in present study.

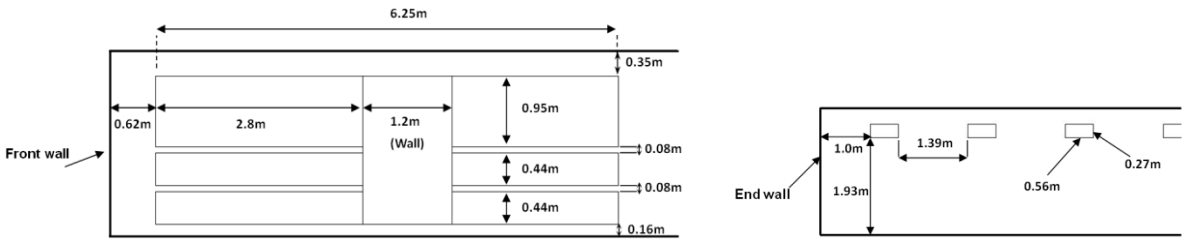

(a) (b)

Figure 2. Dimensions of the (a) side-wall air inlet, (b) side-wall windows

In the house, there were 4 rows of animal occupied zone, each row had 3 tiers of cages as shown in Figure 3a, raising approximate 3,500 laying hens. The size of the cage was length, 2.16 m, width, 0.66 m, height (excluding the manure removing belt), 0.45 m. Each row was 1.36 m apart and the total height of the 3-tier cage was 1.65 m. The bottom of the cage was set 0.5 m high from the ground as shown in Figure 3b.

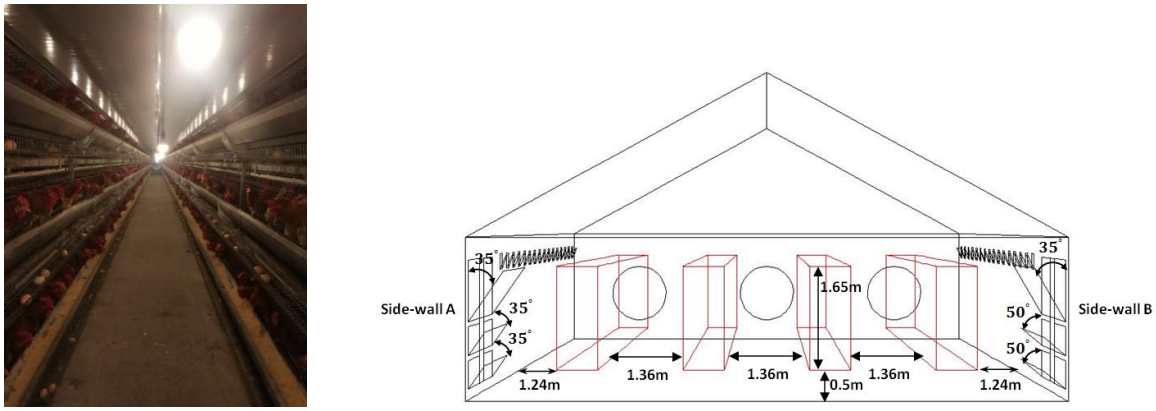

(a) (b)

Figure 3. (a) Photograph of interior of the laying hen house showing the 3-tier animal occupied zone, (b) schematic drawing of the front view of the laying hen house, the animal occupied zone was simplified by red rectangular cuboids.

The cooling pad worked in the condition of negative pressure and was installed just outside each air inlet. The water film supplied by the recyclable water system was formed in the surface of the pad. In order to prevent the cold air, which cooled by the water film, blew directly towards the hens caged in the vicinity of the inlets, the air was designed to enter the house at a pre-set 35° as shown in Figure 3b. However, due to a mechanical failure, 2 flaps at the inlet of the side-wall B could only be set at 50° as shown in Figure 3b. Therefore, special attention was paid when creating the CFD model in order to exactly match the experimental conditions.

2.1.2 Instrumentation

A portable infrared thermometer (Model MT4 MAX, FLUKE, WA) with an accuracy of 1% of the reading or $\pm 1^{\circ}C$ was used to measure the wall temperature including ceiling and floor.

Meanwhile, a portable multi-function high-resolution air velocity meter (Model 9545, TSI, MN) was used to measure the indoor air velocity, air temperature and relative humidity. The detailed specifications of the TSI Model 9545 are given in Table 1. Calibration tests were performed and results demonstrated all the parameters conform to the original manufacturer's specification showing in Table 1.

2.1.3 Measurements

The experimental measurements were conducted in the occupied laying hen house by using the TSI meter, which was placed in 15 different locations at 2 heights: (1) at the height occupied by the birds of the first tier (0.8 m); (2) at the height occupied by the birds of the third tier (1.8 m). The schematic drawing of the measurement positions is shown in Figure 4 and the detailed coordinate information is provided in Table 2 (it should be noted that the origin of the coordinate is shown in Figure 1b).

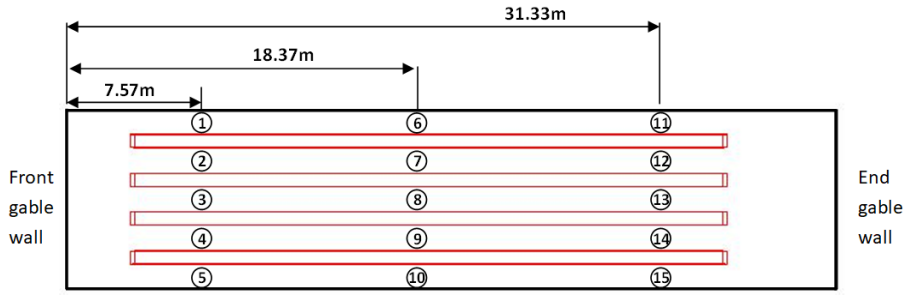

Figure 4. Schematic drawing of the measurement positions in the laying hen house (vertical view)

It should be noted that this small scale experimental-oriented laying hen house is only 40m long and the actual length for the occupied zone is about 32m. The air temperature at the inlets was approximate 20° and the atmosphere temperature is recorded to be about

25.2° during the experiment. Therefore, in order to keep the temperature within the comfort range for all birds caged from the front of the house to the end of the house, the experiment was conducted with only the middle fix-frequency fan in operation and all the side-wall windows fully closed. Applying more fans would result in higher velocity and stronger convectional cooling, which was not suitable especially for those birds caged in the vicinity of the air inlets. Therefore, the experimental measurements were performed with relative low indoor air velocity under the objective experimental conditions. This might be different from some tunnel ventilation studies conducted in large-scale commercial poultry houses with air velocity larger than $2\ \mathrm{m\ s^{-1}}$ (Cheng et al., 2018a). Nevertheless, this relative low air velocity would not affect the validation of the CFD model since the theories of heat transfer and fluid dynamics are the same.

For indoor measurements at the designed points, 3 environmental parameters, which could significantly affect the animal thermal comfort, were measured: they were air temperature, air velocity and relative humidity. The portable TSI meter was fixed on a mobile mast while the mobile mast was situated and moved from point 1 to 15 (see Figure 4) remaining for about 250 seconds at each location. Consequently, air velocity, air temperature and relative humidity inside the test zone were monitored at 30 points. Meanwhile, the above 3 parameters at 5 positions along each side of the air inlet were also measured and the air velocity at the end of the middle fan was measured and recorded. Since the experiments were performed in a poultry house instead of an enclosed laboratory, the parameters at the inlets were measured before and after the experiment in order to detect possible relevant changes in the outside atmosphere condition during the 2-hour measurement process.

For all the measurements taken with the TSI meter, the sampling frequency was 0.2 Hz, and 50 samples were taken at each designed position. In order to reduce measurement noise, the 50 samples were therefore averaged providing standard deviation and the mean value was considered as the reading of the noted time interval.

Since in this study the poultry building was an occupied laying hen house, the interior wall surface temperature distribution was not uniform. Generally speaking, for the tunnel ventilation system the wall surface temperature increases from the front to the end of the house (see Figure 1b). Therefore, in order to set-up the CFD model based on the actual initial experimental condition, wall temperatures at the internal solid surfaces were measured at another empty house with exact the same dimensions and located next to the occupied laying hen house. The wall considered were 2 side walls, the suspended ceiling, the floor, the front wall and the end wall. The measurement was made at five representative points for each surface and the temperature were monitored and recorded before and after the experiment. For wall temperatures, 20 samples for each point were recorded and used to calculate the mean value and the standard deviation.

The indoor concentration of NH_3 and CO_2 during the field measurement was monitored by a gas detector at the end of the house at the animal level and the corresponding recorded value was approximately 3~4ppm and 1300~1400ppm respectively, which was far below the threshold value of 25ppm and 3000ppm respectively (Groot Koerkamp et al., 1998; Zhao et al., 2015). Moreover, according to the literature (ASABE Standards, 1986(R2012)), the optimum ambient temperature for laying hens in terms of maximum egg output is around 24℃ and the weight gain of the broilers during growout show limited difference at the

temperature range of 20℃~30℃. Meanwhile, the performance of the birds is slightly affected by relative humility between 60% and 80%. Therefore, optimizations performed in present study all conformed to these standards. In terms of the determination of ventilation rate, a heat balance of all sources and sinks should be first determined and the readers could refer to ASABE standard (ASABE Standards, 1986(R2012)) for more detailed information about ventilation requirements since this is not the main interest of this study.

2.2 Numerical simulation

2.2.1 Model set-up

In present study, a 3-dimensional simulation of the indoor environment for the occupied laying hen house was carried out by the commercial code Fluent 17.0. The geometry model and mesh were developed by using the commercial code Pointwise V17. The geometry of the laying hen house was modeled using its real dimensions as can be seen in Figure 1b. Since the indoor experimental zone was actually a rectangular cuboid formed by the suspended ceiling, 2 side walls, the front wall, the end wall and the floor, therefore the triangular rooftop (see Figure 1b) was not included in all the CFD simulations. The exhaust fan was considered as a circle of diameter of 1.27 m and only the middle fan was modeled based on the actual experimental condition although there were 3 fans installed at the end wall of the house. Inlets were accurately modeled by means of the coordinates of its corners (see Figure 2a) and the flaps at the 2 inlets were also modeled according to the pre-set degrees as can be seen in Figure 2b. For the validation test, the side-wall windows were not included in the CFD model since all these side-wall windows were kept fully closed during experiments. Nevertheless, the side-wall windows and the corresponding flaps were modeled for the following

optimization studies.

2.2.2 Porous media zone

It is unavoidable to make appropriate approximation when using numerical models to simulate complex 3-dimensional real world problem. Especially in this study, it was unrealistic to model all birds discretely in the geometry modeling. In response to this issue, the porous media model had been applied to simulate the caged laying hen occupied zone, neglecting the feeding system and water supply system. 4 rectangular cuboids (shown in Figure 1b and Figure 2b) were drawn according to the actual dimension to represent the caged laying hen occupied zone, which was later defined as porous media zone in Fluent. The idea of porous media is to add a source term in Navier-Stokes equations. The source term consist of 2 parts, namely, the viscous loss term (Darcy law, the first term on the right-hand side of equation 1) and the inertial loss term (the second term on the right-hand side of equation 1):

$$\frac{\Delta P_i}{\Delta \mathcal{X}_i} = -\left\{\sum_{j=1}^{3} D_{ij}\mu v_j + \sum_{j=1}^{3} C_{ij}\frac{1}{2}\rho|v|v_j\right\} \qquad (1)$$

where, $\Delta P_i/\Delta \mathcal{X}_i$ is the pressure drop per unit length for the i th (x, y or z) direction, Pa m^{-1}; $|v|$ is the magnitude of the velocity, $m\,s^{-1}$; D and C are prescribed matrices for viscous and inertial resistance coefficients, m^{-2} and m^{-1}, respectively; v_j is the inlet air velocity in x, y or z directions, $m\,s^{-1}$; μ is dynamic viscosity of air, $N\,s\,m^{-2}$; ρ is air density, $Kg\,m^{-3}$.

As it can be seen from equation 1, by simplifying the caged laying hen occupied zone into porous media zone, it is crucial to find the correct viscous (D) and inertial (C)

resistance coefficients. According to the recent study performed by Cheng et al. (2018b) who investigated the resistance coefficient by CFD simulation and wind tunnel measurements, it was found that the resistance coefficient was a function of bird geometry, distribution and weight. It should be noted that the density of occupants in Cheng et al. (2018b)'s study was similar to the present study although the bird spatial distribution in the cage might change during the 2-hour experiment. Therefore, Cheng et al. (2018b)'s study provides a reliable data source for present study to set up the porous media zone and the parameters used are shown in Table 3.

The total heat production (THP) for each laying hen was calculated by using equation 2 which was proposed by Chepete and Xin (2001, 2004), where M was the weight of the bird. In present study, the averaged weight (M) for each laying hen was about $2.6\ \mathrm{kg}$ based on the averaged value of 20 samples. Furthermore, in order to simulate the indoor relative humidity distribution, the moisture production of the laying hen was estimated to be $0.94\ \mathrm{mg\ s^{-1}\ kg^{-1}}$ based on Zhai's study (Zhai et al., 2014).

$$\mathrm{THP(W/kg)} = 6.20\mathrm{M}^{-0.29} \quad (2)$$

2.2.3 Grid Convergence study

It is imperative to discretize the space and time when numerical method is used to solve the coupled partial differential equations which describe the key physics. However, due to the limitation of the computer power and time, it is almost impossible to obtain a CFD simulation result that independent of the computational grid especially for such a 3-dimensional flow in a full scale laying hen house. However, it is meaningful to perform a grid convergence study

to ensure the model could represent the actual house and provide reasonable results. Therefore, the widely used uniform Grid Convergence Index (GCI) (Roache, 1994; Roache, 1997) was adopted in this study to quantify the uncertainty of grid convergence. The equations to calculate GCI are expressed as:

$$GCI = 100F_s|\varepsilon|/(r^p - 1) \quad (3)$$

$$\varepsilon = (F_2 - F_1)/F_1 \quad (4)$$

$$r = h_2/h_1 \quad (5)$$

where F_1 is the variable value at point with fine grid and F_2 is the variable value at the same point with coarse grid. According to Roache (1994), for unstructured mesh h_1 and h_2 is the grid number of fine and coarse mesh respectively while for structure mesh h_1 and h_2 is the representative grid size of fine and coarse mesh respectively. F_s is factor of safety equal to 3 based on Rong et al. (2016)'s study. P denotes the numerical scheme order of accuracy, which is 2 for second order scheme. Readers could refer to reference (Roache, 1994; Roache, 1997) for detailed information about GCI calculation. In this study, an unstructured mesh was applied and the chosen variable for GCI study was air velocity. 4 different meshes were analyzed: Mesh A (~ 0.9 millions of cells), Mesh B (~ 1.7 millions of cells), Mesh C (~ 3.2 millions of cells) and Mesh D (~ 5.5 millions of cells). 3 positions in the test zone were picked to examine the grid convergence as shown in Table 4. As demonstrated in Table 4, the GCI values decreases with the increase of cell number for all Points. Especially, for P2 and P3 the Mesh D and Mesh C show negligible differences (GCI is only about 1%). The GCI study reveals that refining the mesh leaded to lower error level as well as lower error estimator. Therefore, considering the accuracy of the calculation and the computing time,

Mesh C was chosen to perform the following CFD simulations.

2.2.4 Boundary conditions

It is noted that quantify and determine the boundary conditions for an animal house could be a difficult task. According to related studies in the literature (Blanes-Vidal et al., 2008; Rojano et al., 2016; Rong et al., 2016; Bustamante et al., 2017), the general way to define the boundary conditions used in numerical study is based on experimental measurements at limited positions, which is considered to be appropriate and best possible approach. Therefore, in present study, the suspended ceiling, the floor, 2 side walls, the end and front walls were represented isothermally at a constant temperature calculated from the mean value of the surface temperature measurements as shown in Table 5. A non-slip condition was imposed for above walls so the fluid velocity at those surfaces was zero. The atmosphere temperature was about $25.2^{\circ}C$ with a relative humidity of approximately 62% and it should be noted that during the 2-hour experimental measurements, the fluctuation of outside atmosphere condition was very limited based on the recordings, therefore Table 5 only shows the parameters measured before the experiments.

4 scenarios with different boundary settings for the inlet and outlet were investigated as there is no agreement in the literature on which combination of boundary conditions is best and different authors applied different boundary conditions for the inlet and outlet (Harral and Boon, 1997; Loomans, 1998; Bjerg et al., 2002; Blanes-Vidal et al., 2008; Rojano et al., 2016). It should be noted that the inlet temperature and relative humidity were kept constant based on experimental measurements (see Table 5) for all scenarios examined and the high

relative humidity at the air inlets results from the evaporative cooling.

In scenario I, the atmosphere pressure condition was used for the 2 side-wall air inlets and the air velocity was applied for the outlet fan. The air velocity value at the outlet was based on the mean value of 3 measured points at the end of the fan (see Table 5). This mean value ($V = 6.21\ m\ s^{-1}$) was also compared with the calculation result of the total ventilation rate divided by fan's area showing less than 3% discrepancy. In scenario II, velocity inlet was assumed to be equally distributed over all inlet areas and the value is approximately $0.76\ m\ s^{-1}$ as shown in Table 5. The outlet condition was set as atmosphere pressure outlet. In scenario III, the inlet condition was set as atmosphere pressure inlet and the pressure outlet value was calculated from the air velocity by using Bernoulli equation since the air was considered to be an idea, incompressible fluid. Finally in scenario IV, air velocity was applied again for the inlet condition while airflow rate calculated from the air velocity and fan's area was used as the outlet condition. The 4 scenarios examined are summarized in Table 6.

2.2.5 Turbulence model and general settings

The realizable k-ε turbulence model were used in CFD simulation since k-ε turbulence model was widely used in the literature to study the indoor flow and environmental parameters for livestock (Norton et al., 2007), and the realizable k-ε turbulence model had improvements on the prediction for flow rotation, recirculation and boundary separation (Rong et al., 2016) which were expected in this study. Furthermore, standard wall functions were applied to the model with special attention paid to the parameter of y^* since for high Reynolds number k-ε model, standard wall function are effective only when $30 < y^* <$

300. Readers could refer to reference (Rong, 2016) for more detailed information about wall functions. It was assumed that the CFD simulation was an incompressible, turbulent, 3-dimensional steady flow. Air properties were considered to be constant. Table 7 summaries the other settings used for all CFD simulations. The residual for energy equation arrived at 10^{-7} and the residual for other equations arrived at 10^{-5} for all the CFD simulation performed in present study.

2.3 Regression model

Although the CFD model could be validated directly by comparing the simulation results with the experimental measurements, there is no proper criterion to judge which boundary setting for the inlet and outlet is better (see Table 6). Therefore, a stepwise logistic regression analysis was performed by using the commercial software SPSS (Version 20). This analysis can supply information to determine the differences between different boundary conditions regarding the agreement between measured and CFD simulated results, and also analyze the effect on this agreement of the position inside the building (x, y, z). Meanwhile, the results of this analysis could also be used to adjust the CFD simulated results to take into account the experimental data. The CFD velocity values at the coordinates where the indoor measurements were taken were obtained by creating 'fictitious' sensors in CFD model and the data was then exported to the SPSS for regression analysis.

The stepwise logistic regression analysis used a second-order multiple regression model with independent variable defined as the sensor position in the test zone and dependent variable defined as the relative error which is shown in equation 6. The interactions between

all independent variable were also automatically investigated by the regression model.

$$E_r = |(V_{CFD} - V_{EXP})/V_{EXP}| \quad (6)$$

where V_{EXP}（$m\ s^{-1}$） is the experimental measured velocity at each designed position and V_{CFD}（$m\ s^{-1}$） is the air velocity simulated by CFD model at the corresponding position.

Finally, the Hosmer–Lemeshow test (Hosmer and Lemeshow, 2013) was conducted based on the regression analysis, which was a statistical test for goodness of fit for logistic regression models, to evaluate the simulated results from the 4 different boundary scenarios using the Chi-square (χ^2) index. Lower value of χ^2 indicates a better fit of CFD results on the experimental measurements.

2.4 Optimization of air inlet configurations

It is generally acknowledged that the indoor air velocity and movement (or flow pattern) play important roles in affecting the convective animal heat losses. The configuration of the air inlets therefore becomes important. Uniformity of indoor air velocity in the caged laying hen occupied zone would lead to a uniform convectional cooling and prevent excessive (or inadequate) local convective heat losses, which contributes to the increased bird mortality and decreased productivity. In present study, the field measurements were performed in a poultry house equipped with 2 side-wall inlets, which located at the front end of the house as shown in Figure 1b. However, there was no guarantee that side-wall air inlets were the optimum configuration. Accordingly, 3 different air inlet configuration strategies were examined and compared with the original design by using the validated CFD model. In order to make the comparison meaningful, all the CFD simulations were performed with the same

environmental parameters as shown in Table 5 and the side-wall windows were kept closed since the effect of side-wall windows would be studied separately. The air inlets were placed at different positions of the poultry house but the total areas of the inlets were kept the same as the original design for direct comparison.

Case I was the original experimental condition with 2 side-wall inlets located at the front end of the house (see Figure 1). In Case II, part of the side-wall inlets were moved to the front wall. In Case III, the inlet was placed at the front wall with the same total inlet area. Moreover, in case IV the inlet configuration consisted of front-wall inlet and side-wall inlet which located at the middle of the house. Details of the cases investigated are summarized and illustrated in Table 8 and Figure 5. It should be noted that the above optimization strategies only provide the possible methods to improve the indoor environment, further studies could be performed to compare more configurations and combinations to provide detailed information about the best inlet confirmation for poultry houses.

The key focuses for each case investigated were the indoor flow uniformity (flow pattern), temperature and relative humidity distribution which would directly affect the birds' thermal comfort. A more uniform flow with lower temperature difference between the front and the end of the house is expected for the better inlet configuration.

Schematic drawing of the optimized inlet configuration	CASE	Remarks
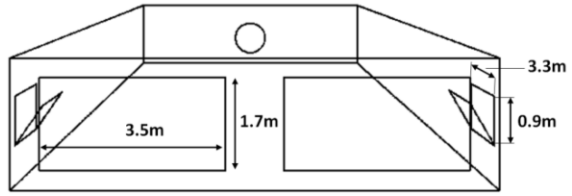	**Case II**	Area ratio of side-wall inlets to front wall inlets is 2:1
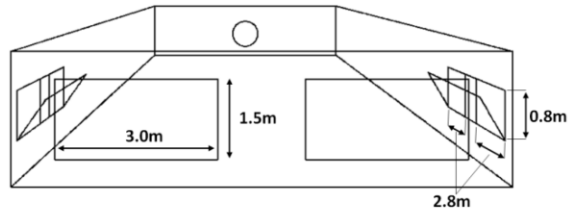	**Case II**	Area ratio of side-wall inlets to front wall inlets is 1:1
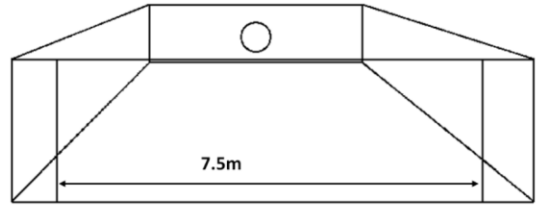	**Case III**	
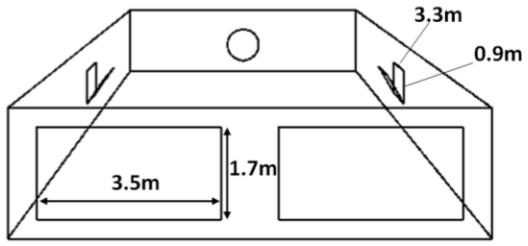	**Case IV**	Area ratio of middle side-wall inlets to front wall inlets is 1:2
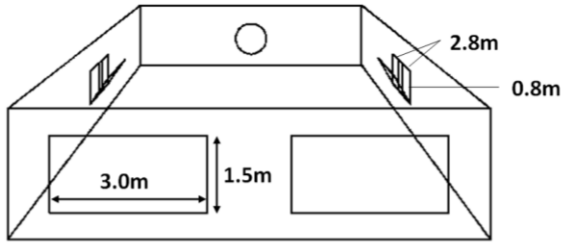	**Case IV**	Area ratio of middle side-wall inlets to front wall inlets is 1:1
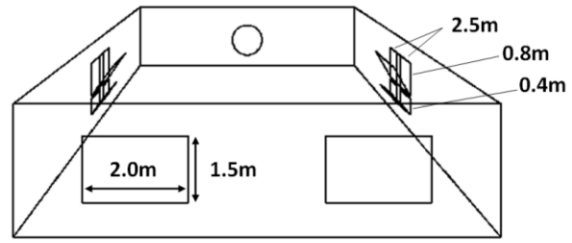	**Case IV**	Area ratio of middle side-wall inlets to front wall inlets is 1:2

Figure 5 Schematic drawing of the optimized inlet configurations with dimensions

3. RESULTS AND DISCUSSION

3.1 Model validation

3.1.1 Statistical analysis

According to the environmental conditions measured before the experiments (see Table 5), 4 CFD simulations (Scenario I, II, III and IV) were performed. The CFD velocity values at the coordinates where the indoor measurements were taken were obtained for each scenario and the Hosmer–Lemeshow test was conducted to evaluate the goodness of fit. As illustrated in Table 9, all 4 scenarios examined were not significant ($p > 0.05$) in Hosmer–Lemeshow test, and the calculated Chi-square χ^2 were all lower than the limitation of $15.5(= \mathrm{CHIINV}(0.05, \mathrm{df}))$ suggesting a good fit. Scenario III presented the lowest χ^2 ($\chi^2 = 7.555$) comparing with scenario I ($\chi^2 = 8.762$), scenario II ($\chi^2 = 10.126$) and scenario IV ($\chi^2 = 10.868$). Therefore, the boundary settings for scenario III, which were pressure inlet and pressure outlet, were selected for the following CFD studies.

9 position independent variables were utilized in the stepwise logistic regression analysis, they were x, y, z, x^2, y^2, z^2, xy, xz, yz. The final fitted model involved 8 independent variables as shown in Table 10, indicating the relative error (E_r) was significantly different depending on the location of the position being studied. The coefficient of each independent variable enables the CFD simulation results to be modified by taking the experimental data into consideration although this is not the main interest of present study.

3.1.2 CFD validation

3 parameters (air temperature, air velocity and relative humidity) were measured at the 30

designed positions during the experiment and the CFD results at the corresponding positions were compared and illustrated in Table 11, Table 12 and Table 13.

As it can be seen in Table 11, the air temperatures predicted by the CFD model at the designed positions match the experimental measurements in general. Considering the absolute error ($T_{CFD} - T_{EXP}$) as a criterion, 22 out of 30 predicted values differ by less than $1^{\circ}C$. Meanwhile the relative error E_r indicates that 25 out of 30 predicted values are less than 5%, indicating a good agreement. Relative larger discrepancies are found at the end of the animal occupied zone where high air temperature is expected.

Furthermore, the velocity value predicted by the CFD model is shown in Table 12. It should be noted that in order to avoid the large relative error which could arise when air velocities are very small, previous studies (Harral and Boon, 1997; Zhao et al., 2003; Blanes-Vidal et al., 2008) usually expressed the differences between measured and simulated air velocity in terms of E_b, that is, as a percentage of the mean air velocity at the inlets (V_0). Since in present study, the indoor air velocity range is relative small ($0.2\ m\ s^{-1} \sim 0.8\ m\ s^{-1}$) therefore index E_b is adopted here. The maximum absolute error observed is about $0.08\ m\ s^{-1}$ with a $E_b = 11.4\%$ at sensor number 4. However, as it is shown in Figure 4, the sensor number 4 is at the front of the occupied zone where in the vicinity of the side-wall inlets. This high discrepancy is probably related to the large turbulence and flow disturbance resulting from 2 strands of airflow (from side-wall inlet A and inlet B) collide at the middle of the house. In 27 out of 30 points, the differences between measured and predicted air velocities, expressed as E_b are less than 10%, and in 15 out of 30 points, the differences are less than 5%. Take the complexity of the flow into consideration, the above results can

be considered satisfactory according to Harral et al.(1997), Blanes-Vidal et al.(2008) and Cheng et al., 2018a.

Regarding the relative humidity predicted by the numerical model, the results demonstrate good agreement with the experimental measurements as shown in Table 13. All the relative errors are less than 10% and in 18 out of 30 points, the differences of relative error are less than 5%. It should be noted that the simulated results (RH_{CFD}) always underestimate the relative humidity, resulting in a negative absolute error. Especially, the large discrepancies occur at the end of the occupied zone (sensor number 16 to 24). One possible explanation is that although the CFD model has taken the moisture production from the birds into consideration, the manure would also contribute to the increase of relative humidity and this is not included in the model. Therefore, the experimental measurements show slightly higher relative humidity at most of the positions measured.

In conclusion, by comparing the CFD results with experimental measurements in terms of air temperature, air velocity and relative humidity at the designed 30 positions, the CFD simulation shows good agreement with the experimental results especially taking the complexity of the flow into account. The CFD model provides an effective and efficient method to predict the distribution and dynamic change of indoor environmental parameters.

3.2 Optimization and discussion

Preliminary investigations about the optimum air inlet configurations and effective utilization of side-wall windows are provided in this study to shed some lights on the future optimization of the tunnel ventilation systems.

3.2.1 Optimum air inlet configurations

- Case I, II and III

Illustrative planes were obtained by using isosurfaces and the parameter of vorticity magnitude, which describes the local spinning motion of a continuum, is used to indirectly show the non-uniformity level of the indoor air movement. It should be noted that the illustrative planes were examined at different heights but showing the same trend of changes, so results at height $Y = 1.8\ \mathrm{m}$ will be used for most of the following sections.

As it can be seen in Figure 6, Case I demonstrates a considerable high level of vorticity magnitude at the front of the poultry house indicating a non-uniformity of local air movement. This strong turbulent flow is due to the collision of air at the central of the house, which entering the building from the 2 side-wall inlets. In terms of convectional cooling, the local strong turbulent flow contributes to unnecessary excessive heat exchange, which would lead to excessive animal heat losses. By moving part of the side-wall inlets to the front wall, the vorticity magnitude at the front of the house is significantly decreased as shown by Case II in Figure 6b and 6c. When the air inlets are all placed at the front wall, a good uniform flow is presented by Case III (Figure 6d) with limited vorticity magnitude resulting from the animal occupied zone.

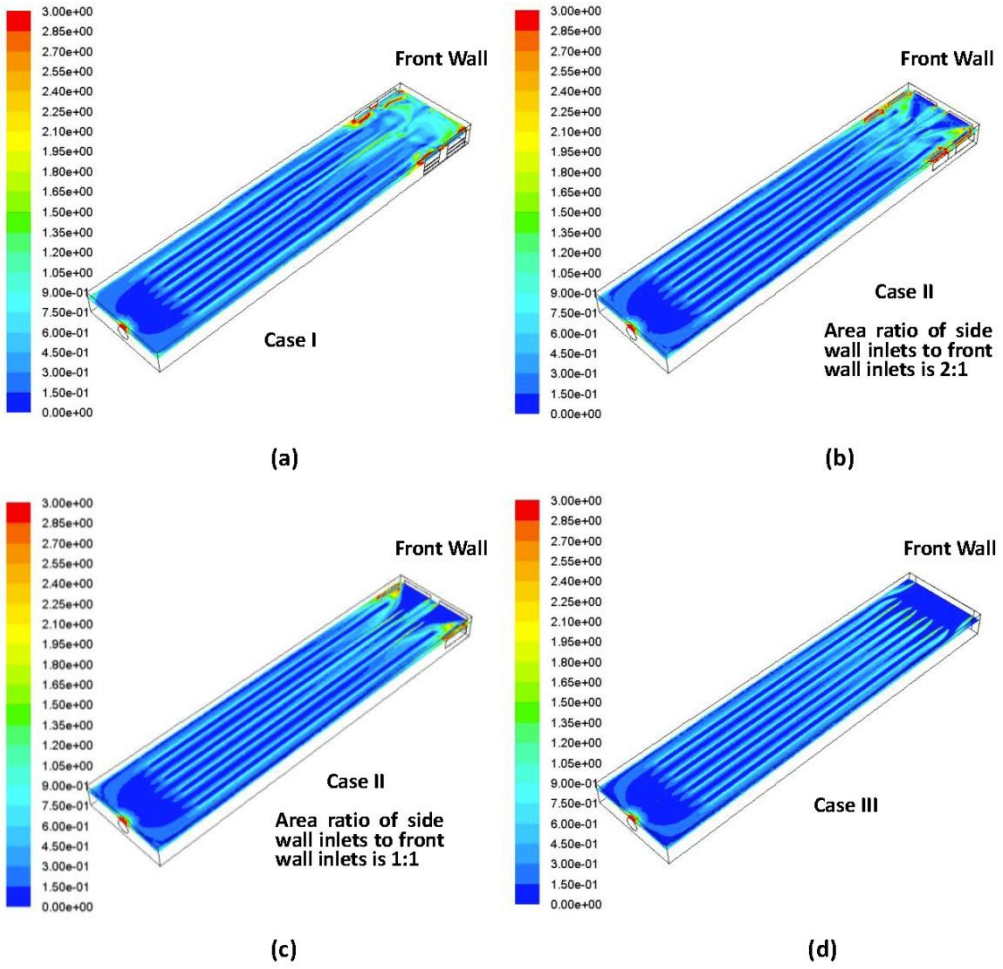

Figure 6. Vorticity magnitude in the plane of height $Y = 1.8$ m for (a) Case I; (b),(c) Case II and (d) Case III. Unit: s^{-1}.

Furthermore, since the indoor temperature will directly affect the animal thermal comfort, the temperature distributions are illustrated in Figure 7. Comparing the isosurfaces of Case I and Case III, an interesting result can be found that the front-wall inlets configuration (Case III) not only shows a uniform indoor temperature gradient at the front of the house but also demonstrate a lower temperature zone at the end of the house. With a high turbulent flow as in Case I, the birds caged at the front of the house experience excessive heat losses due to the strong convectional cooling comparing with that in Case III. The Figure 7b clearly shows that the aisle temperature at the front of the occupied zone is only approximately 293 K (20°C)

in Case III while it is about 295 K (22°C) in Case I (Figure 7a). Meanwhile, the Figure 7b shows that in Case III the temperature at the front of the animal occupied zone is about 299 K (26°C). But in comparison, the temperature at the front of the animal occupied zone in Case I is only about 295 K (22°C) indicating that the heat is carried away by the cold turbulent flow. As shown in Case I the larger heat exchange at the front of the animal occupied zone increases the flow temperature and finally exacerbates the heat gradient at the end of the house. Table 14 provides detailed information about the temperature values at the end of the occupied zone at sensor No.11~15 (defined in Figure 4) for different inlet configurations. An approximately 0.5°C drop of temperature at the end of the animal occupied zone is predicted by improving the uniformity of indoor air movements (Case III), which further demonstrating and supporting the above conclusions.

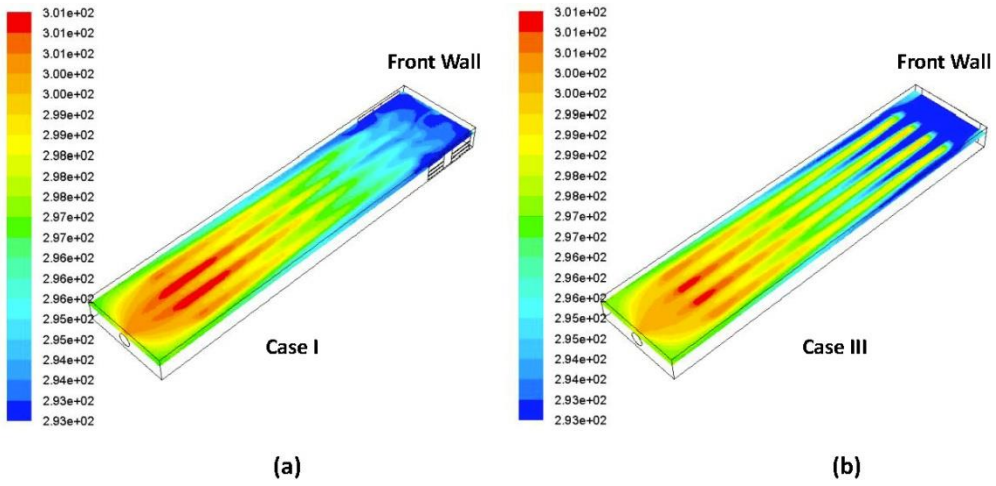

Figure 7. Temperature distribution for (a) Case I and (b) Case III. Isosurfaces in the plane of height Y = 1.8 m. Unit: Kelvin, K.

- Case IV

For poultry houses with tunnel ventilation system, the temperature difference between the front and end of the house should be kept small especially for large-scale poultry farms with building length larger than 100 m. One possible method to achieve this goal is to increase the indoor air velocity and flow rate, which carries the heat away by fast air movement using large amount of energy. Nevertheless, from the standing point of ventilation design, this study investigates another way to reduce the high temperature expected at the end of the poultry house by adding side-wall air inlets at the middle of the building. This ventilation configuration consists of front-wall inlets and middle side-wall inlets, all equipped with the evaporative cooling systems. The simulated indoor temperature distribution is shown in Figure 8.

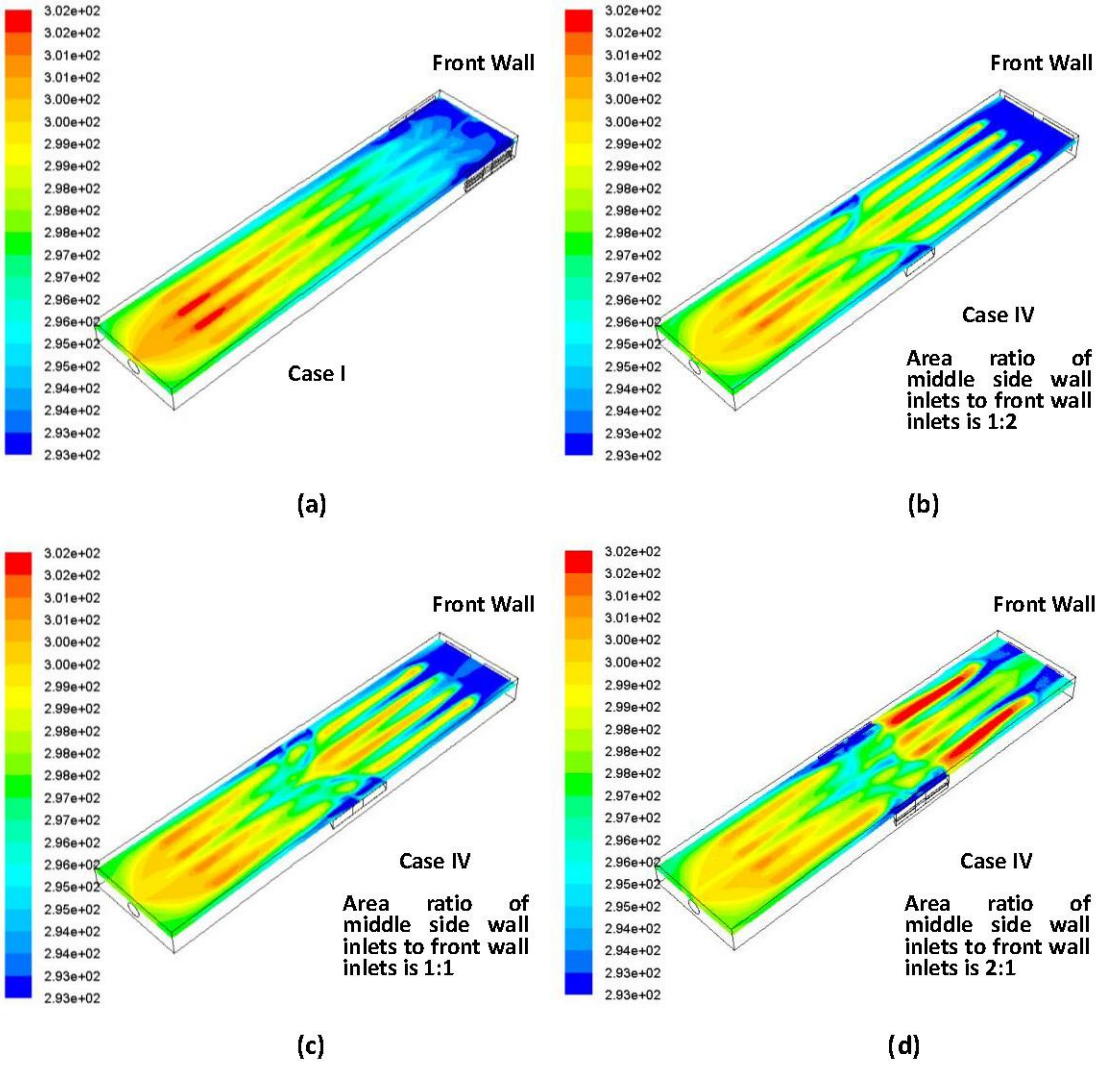

Figure 8. Temperature distributions for (a) Case I and (b), (c), (d) Case IV. The total area of air inlets are the same for each cases. Isosurfaces in the plane of height $Y = 1.8$ m. Unit: Kelvin, K.

By moving part of the inlets to the middle of the side wall, the cold air from the front wall cools the front half of the animal occupied zone while the cold fresh air that enters from the middle side-wall inlets cools the end half of the house as it is clearly demonstrated in Figure 8b and 7c. Comparing with the original ventilation system (Case I, Figure 8a), the temperatures at the end of the animal occupied zone decreases from approximate

301 K (28°C) in Case I to about 299 K (26°C) in Case IV and no extra energy is used.

However, it is also noted that there is an optimum balance for the area ratio of front-wall inlets to the middle side-wall inlets. The Figure 8d clearly illustrates that by further reduce the area of front-wall inlets, the heat generated by the birds at the front part of the occupied zone cannot be carried away efficiently by sufficient air flow resulting in high temperatures predicted by the model. Therefore, according to this preliminary study, moving half of the inlets area to the middle of the side wall as shown in Figure 8c seems to be a good choice for large-scale poultry farms with long buildings.

3.2.2 Side-wall windows

For the majority of tunnel-ventilated poultry houses in China, side-wall windows were used to regulate the indoor climate. In this study, the performance of these side-wall windows is examined (fully open) and comparison is made with the houses without side-wall windows. The environmental parameters for all CFD studies were kept the same as shown in Table 5 in order to make direct comparison.

As illustrated in Figure 9, the isosurfaces in the planes of $Z = 10$ m, $Z = 20$ m and $Z = 30$ m clearly demonstrate that the side-wall windows have significant effects on the indoor temperature gradient. For poultry houses with side-wall windows open, part of the hot outside air will not be cooled by the water film installed at the air inlets but directly enters the house through the windows and then considerably increases the temperature at the end of the animal occupied zone (Figure 9b). Meanwhile, as shown in Figure 10 the side-wall windows also have significant effects on the indoor relative humidity distribution. Although the water film

cools the air before it enters the poultry house, the air humidity becomes extreme high which also might affect the animal thermal comfort and productivity under certain circumstances. In comparison, the relative humidity of outside air is only about 62% as shown in Table 5, and the predicted relative humidity at the end of the animal occupied zone is decreased from about 70% for the case without side-wall windows to 55% for the case with side-wall windows as shown in Figure 10.

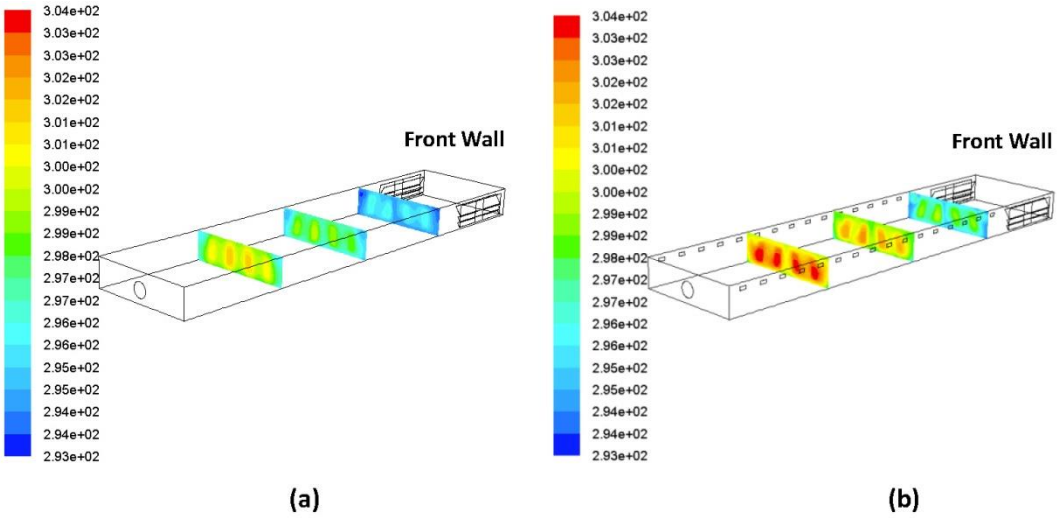

Figure 9. The temperature isosurfaces in the planes of length $\mathrm{Z} = 10$ m, $\mathrm{Z} = 20$ m, $\mathrm{Z} = 30$ m for (a) the poultry house without side-wall window and (b) the poultry house with side-wall windows. Unit: Kelvin, K. It should be noted that the atmosphere temperature is 298.2 K (25.2°C).

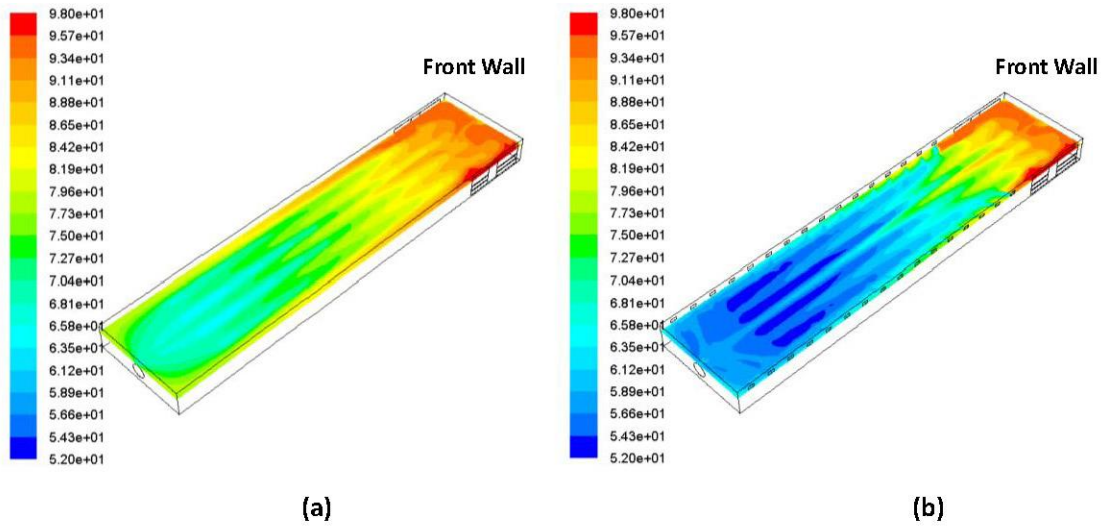

Figure 10. The relative humidity distribution in the plane of height $Y = 1.8\,\mathrm{m}$ for (a) the poultry house without side-wall window and (b) the poultry house with side-wall windows. Atmosphere relative humidity is 62%.

Based on the climate conditions in Chengdu, China, some preliminary suggestions were provided here for tunnel-ventilated poultry houses to effectively use the side-wall windows:

- In summer, it is better to keep the side-wall windows closed all the time since the atmosphere temperature is high ($25^{\circ}\mathrm{C}\sim35^{\circ}\mathrm{C}$) and limited gains could be obtained by using the side-wall windows.
- In winter, since the outside temperature is low (($0^{\circ}\mathrm{C}\sim15^{\circ}\mathrm{C}$), the side-wall windows could be applied with the fans to regulate the indoor temperature and humidity at some pre-set time intervals.
- In spring and autumn, the side-wall windows could be controlled effectively with the environmental monitoring system. With a modest outside climate (temperature is $15^{\circ}\mathrm{C}\sim25^{\circ}\mathrm{C}$), the side-wall windows could be fully or partially open to ensure the indoor temperature and relative humidity both within the animal comfort range.

4. CONCLUSION

In present study, a 3-dimensional CFD model was build based on the real dimensions of a laying hen house, which was equipped with tunnel ventilation system. In order to validate the CFD model, the simulation results of air velocity, air temperature and relative humidity at 30 positions inside the building were compared with the filed measurements.

4 different boundary conditions were applied in the CFD model and statistical analysis was then performed to determine the agreement between simulation results and experimental measurements. The Chi-square χ^2 index was used to evaluate the goodness of fit for different boundary conditions and the combination of pressure inlet and pressure outlet, which demonstrated a minimum χ^2, was finally chosen as the simulation setting in this study.

Illustrative planes obtained from the validated CFD model were used to investigate the possible optimum air inlet configurations for tunnel-ventilated poultry houses. It was found that the original side-wall air inlet configuration would lead to strong turbulent flow at the front of the house, which contributed to the excessive convective heat losses for the birds caged at the front area. Meanwhile, the heat would be carried by the air movement from the front to the end of the house and further exacerbated the high temperature distribution expected at the end. By moving part of the inlets to the front wall or placing all the air inlets at the front wall of the house, the uniformity of indoor air movement was significantly increased and a maximum of about $0.5^{\circ}C$ temperature drop at the end of the animal occupied zone could be achieved.

In order to reduce the temperature differences between the front and end of the house, studies were conducted to investigate the effects of placing the air inlets at the middle of

house. The CFD simulation results indicated that proper area of air inlets installed at the middle of the side wall could considerately decrease the high temperature expected at the end of the building without increasing the ventilation rate and using extra energy. However, when the total area of air inlets were kept the same, further increasing the area of air inlets at the middle of the side wall would lead to insufficient cold air enter from the front-wall inlets. Therefore, the heat generated from the front of the animal occupied zone could not be carried away efficiently by the cold air resulting in high temperatures predicted. Based on the preliminary results from this study, moving half of the inlet area to the middle of the side wall seemed to be a good choice for large-scale poultry farms with long buildings.

The CFD model also demonstrated that the side-wall windows would significantly affect the indoor air temperature and relative humidity distribution. However, from another point of view, the side-wall windows could be applied with the environmental monitoring system to regulate the indoor climate effectively. Some preliminary suggestions were provided in this study for different temperature range throughout the year.

All in all, this paper provides scientific research results and data for studying the performance of tunnel ventilation system used in poultry houses. Simulation predictions and suggestions contribute to the understanding and design of the tunnel ventilation system, which is scarce in the literature.

5. ACKNOWLEDGEMENTS

This work was funded by the national key research and development project (No. 2016YFD0500510); Sichuan Science and Technology Program (No. 2018JY0595); the national science and technology support planning project (No. 2015BAD03B03); the province key technologies R&D program of livestock and poultry breeding programs of Sichuan province (No. 2016NYZ0043).

REFERENCES

Allocca, C., Chen, Q., Glicksmann, L.R., 2003. Design analysis of single-sided natural ventilation. Energy Build. 35:785-795.

ASABE Standards, 1986(R2012). ASAE EP270.5 DEC1986(R2012), Design of Ventilation Systems for Poultry and Livestock Shelters. St. Joseph, MI 49085-9659, USA.

Bjerg, B., Cascone, G., Lee, I.B., Bartzanas, T., Norton, T., Hong, S.W., Seo, I.H., Banhazi, T., Liberati, P., Marucci, A., Zhang, G., 2013. Modelling of ammonia emissions from naturally ventilated livestock buildings. Part 3: CFD modelling. Biosyst. Eng. 116:259-275.

Bjerg, B., Svidt, K., Zhang, G., Morsing, S., Johnsen, J.O., 2002. Modeling of air inlets in CFD prediction of airflow in ventilated animal houses. Comput. Electron. Agric. 34:223-235.

Blanes-Vidal, V., Guijarro, E., Balasch, S., Torres, A.G., 2008. Application of computational fluid dynamics to the prediction of airflow in a mechanically ventilated commercial poultry building. Biosyst. Eng. 100:105-116.

Bustamante, E., Calvet, S., Estelles, F., Torres, A.G., Hospitaler, A., 2017. Measurement and numerical simulation of single-sided mechanical ventilation in broiler houses. Biosyst. Eng. 160:55-68.

Bustamante, E., Garcia-Diego, F.J., Calvet, S., Torres, A.G., Hospitaler, A., 2015. Measurement and numerical simulation of air velocity in a tunnel-ventilated broiler house. Sustainability. 7:2066-2085.

Bustamante, E., Garciadiego, F.J., Calvet, S., Estelles, F., Beltran, P., Hospitaler, A., 2013. Exploring Ventilation Efficiency in Poultry Buildings: The Validation of Computational Fluid Dynamics (CFD) in a Cross-Mechanically Ventilated Broiler Farm. Energies. 6:2605-2623.

Calvet, S., Cambralopez, M., Blanesvidal, V., Estelles, F., Torres, A.G., 2010. Ventilation rates in mechanically-ventilated commercial poultry buildings in Southern Europe: Measurement system development and uncertainty analysis. Biosyst. Eng. 106:423-432.

Cheng, Q., Li, H., Rong, L., Feng, X., Zhang, G., Li, B., 2018a. Using CFD to assess the influence of ceiling deflector design on airflow distribution in hen house with tunnel ventilation. Computers and Electronics in Agriculture 151:165-174.

Cheng, Q., Wu, W., Li, H., Zhang, G., Li, B., 2018b. CFD study of the influence of laying hen geometry, distribution and weight on airflow resistance. Comput. Electron. Agric. 144:181-189.

Chepete, H., Xin, H., 2001. Heat and Moisture Production of Poultry and Their Housing Systems – A Literature Review. Livestock Environment VI: Proc. 6th International Symp., Louisville, Kentucky, USA.

Chepete, H., Xin,H., 2004. Heat and Moisture Production of Poultry and Their Housing Systems: Molting Hens. ASHRAE Trans. 110.

Groot Koerkamp, P.W.G., Metz, J.H.M., Uenk, G.H., Phillips, V.R., Holden, M.R., Sneath, R.W., Short, J.L., White, R.P.P., Hartung, J., Seedorf, J., Schroder, M., Linkert, K.H., Pedersen, S., Takai, H., Johnsen, J.O., Wathes, C.M., 1998. Concentrations and Emissions of Ammonia in Livestock Buildings in Northern Europe. Journal of

Agricultural Engineering Research. 70:79-95.

Harral, B., Boon, C.R., 1997. Comparison of predicted and measured air flow patterns in a mechanically ventilated livestock building without animals. Agricultural Engineering Reserch. 66:221-228.

Hosmer, D.W., Lemeshow, S., 2000. Pages 91-142 in Logistic Regression. Applied Logistic Regression. Wiley-Interscience Publication, New York.

Lee, I., S. Sase, Sung, S.H., 2007. Evaluation of CFD accuracy for the ventilation study of a naturally ventilated broiler house. Jpn. Agric. Res. Q. 41:53-64.

Lee, I., You, B.K., Choi, K.H., Jeun, J.G., Kim, G.W., 2003. Study of internal climate of naturally and mechanically ventilated broiler houses. ASAE meeting Paper No. 034060. ASAE, Las Vegas, USA.

Loomans, M., 1998. The measurement and simulation of indoor air flow. Phd Diss., Technische Universiteit Eindhoven, Eindhoven.

Norton, T., Grant, J., Fallon, R., Sun, D.W., 2009. Optimising the ventilation configuration of naturally ventilated livestock buildings for improved indoor environmental homogeneity. Build. Environ. 45:983-995.

Norton, T., Grant, J., Fallon, R., Sun, D.W., 2010. A computational fluid dynamics study of air mixing in a naturally ventilated livestock building with different porous eave opening conditions. Biosyst. Eng. 106:125-137.

Norton, T., Sun, D.W., Grant, J., Fallon, R., Dodd, V., 2007. Applications of computational fluid dynamics (CFD) in the modelling and design of ventilation systems in the agricultural industry: A review. Bioresour. Technol. 98:2386-2414.

Oloyo, A., 2018. The Use of Housing System in the Management of Heat Stress in Poultry Production in Hot and Humid Climate: a Review. Poultry Science Journal. 6:1-9.

Rahman, M., Chu, C.M., Kumaresen, S., Yan, F.Y., Kim, P.H., Mashud, M., Rahman, M.S., 2014. Evaluation of the Modified Chimney Performance to Replace Mechanical Ventilation System for Livestock Housing. Procedia Eng. 90:245-248.

Roache, P., 1994. Perspective: a method for uniform reporting of grid refinement studies. J. Fluids. Eng. 116:405-413.

Roache, P., 1997. Quantification of uncertainty in computational fluid dynamics. Annu. Rev. Fluid Mech. 29:123-160.

Rojano, F., Bournet, P.E., Hassouna, M., Robin, P., Choi, C.Y., Kacira, M., 2014. Test of two different schemes through CFD to include heat and mass transfer induced by animals inside a broiler house. International Conference for Agricultural Engineering, Zurich, Switzerland.

Rojano, F., Bournet, P.E., Hassouna, M., Robin, P., Kacira, M., Choi, C.Y., 2015. Modelling heat and mass transfer of a broiler house using computational fluid dynamics. Biosyst. Eng. 136:25-38.

Rojano, F., Bournet, P.E., Hassouna, M., Robin, P., Kacira, M., Choi, C.Y., 2016. Computational modelling of thermal and humdity gradients for a naturally ventilated poultry house. Biosyst. Eng. 151:273-285.

Rong, L., Liu, D., Pedersen, E.F., Zhang, G., 2014. Effect of climate parameters on air exchange rate and ammonia and methane emmissions from a hybrid ventilated dairy cow building. Energy Build. 82:632-643.

Rong, L., Liu, D., Pedersen, E.F., Zhang, G., 2015. The effect of wind speed and direction and surrounding maize on hybrid ventilation in a dairy cow building in Denmark. Energy Build. 86:25-34.

Rong, L., Nielsen, P.V., Bjerg, B., Zhang, G., 2016. Summary of best guidelines and validation of CFD modeling in livestock buildings to ensure prediction quality. Comput. Electron. Agric. 121:180-190.

Sun, H., Stowell, R.R., Keener, H.M., Michel, F.C., 2002. Two-dimensional computational fluid dynamics (CFD) modeling of air velocity and ammonia distribution in a high-rise hog building. Trans. ASAE. 45:1-10.

Tong, X., Hong, S-W., Zhao, L., 2019. CFD modelling of airflow pattern and thermal environment in a commercial manure-belt layer house with tunnel ventilation. Biosyst. Eng. 178:275-293.

Wheeler, E., Zajaczkowski, J.L., Saheb, N.C., 2003. Field evaluation of temperature and velocity uniformity in tunnel and conventional ventilation broiler houses. Appl. Eng. Agric. 19:367-377.

Xin, H., Berry, I.L., Taler, G.T., Barton, T.L., 1994. Temperature and humidity profiles of broiler houses with experimental conventional and tunnel ventilation systems. Applied engineering in agriculture 10(4): 535-542 10:535-542.

Zajicek, M., Kic, P., 2013. Simulation of the broiler house ventilation. Scientia Agriculturae Bohemica 1:32-37.

Zhai, Y., Zhang, X., Yang, J., 2014. Study of the flow filed, air temperature and relative humidity for a poultyr house with longnitudinal ventilation system. Jiangsu Agricultural

Sciences 3:337-342. doi 10.15889/j.issn.1002-1302.2014.03.030

Zhao, B., Li, X., Yan, Q., 2003. A simplified system for indoor airflow simulation. Build. Environ. 38:543-552.

Zhao, Y., Shepherd, T.A., Li, H., Xin, H., 2015. Environmental assessment of three egg production systems–Part I: Monitoring system and indoor air quality. Poultry Science. 94:518-533.

APPENDIX

Nomenclature

Parameter	Definition	Unit
C	Matrices for inertial resistance coefficients	m^{-1}
Cp	Specific heat capacity of air	$J\ kg^{-1}\ K^{-1}$
D	Matrices for viscous resistance coefficients	m^{-2}
E_r	Relative error	
E_b	The differences between measured and simulated air velocity as a percentage of the mean air velocity at the inlets	$N\ s\ m^{-2}$
F	variable value at certain point	
F_s	Factor of safety	
h	Grid number	
K	Kelvin temperature	K
P	Numerical scheme order of accuracy	
V_0	Air velocity at the inlets	
$\Delta P_i/\Delta \mathcal{X}_i$	Pressure drop per unit length for the i th (x, y or z) direction	$Pa\ m^{-1}$
$\lvert v \rvert$	The magnitude of the velocity	$m\ s^{-1}$
χ^2	Chi-square	
df	Degree of freedom	
℃	Celsius temperature	

Acronym	Definition	Unit
CFD	Computational Fluid Dynamics	
RH	Relative Humidity	
Hz	Hertz	Hz
THP	Total Heat Production	W/kg
GCI	Grid Convergence Index	

Tables

Table 1 - Specifications of Model 9454, TSI

	Velocity Probe	Temperature Probe	Relative Humidity Probe
Range	0 to 30 m s^{-1}	−10 to 60 °C	0 to 99% RH
Accuracy	±3% of reading or ±0.015 m s^{-1}	±0.3 °C	±3% RH
Resolution	0.01 m s^{-1}	0.1 °C	0.1% RH

Table 2 - The coordinate of the measurement positions

Sensor Number	X-coordinate (m)	Y-coordinate (m)	Z-coordinate (m)
1	8.58	1.80	7.57
2	6.62	1.80	7.57
3	4.60	1.80	7.57
4	2.58	1.80	7.57
5	0.62	1.80	7.57
6	0.62	1.80	18.37
7	2.58	1.80	18.37
8	4.60	1.80	18.37
9	6.62	1.80	18.37
10	8.58	1.80	18.37
11	8.58	1.80	31.33
12	6.62	1.80	31.33
13	4.60	1.80	31.33
14	2.58	1.80	31.33
15	0.62	1.80	31.33
16	8.58	0.80	31.33
17	6.62	0.80	31.33
18	4.60	0.80	31.33
19	2.58	0.80	31.33
20	0.62	0.80	31.33
21	0.62	0.80	18.37
22	2.58	0.80	18.37
23	4.60	0.80	18.37
24	6.62	0.80	18.37
25	8.58	0.80	18.37
26	8.58	0.80	7.57
27	6.62	0.80	7.57
28	4.60	0.80	7.57
29	2.58	0.80	7.57
30	0.62	0.80	7.57

Table 3 - Resistance coefficient for porous media zone

X-direction		Y-direction		Z-direction	
D_x , m^{-2}	C_x , m^{-1}	D_y , m^{-2}	C_y , m^{-1}	D_z , m^{-2}	C_z , m^{-1}
11381.20	0.82	22005.50	3.23	7121.50	2.27

Table 4 - GCI calculated for velocity values of grid ratio r

Points	Location			GCI		
	X	Y	Z	r =1.56	r =1.23	r =1.19
P1	4.6	1.2	10.0	31.10%	22.02%	6.47%
P2	4.6	0.5	20.0	6.02%	3.56%	1.15%
P3	4.6	2.0	30.0	12.49%	6.32%	1.61%

Note: r = 1.19 is the mesh ratio from Mesh D to Mesh C, r = 1.23 is the mesh ratio from Mesh C to Mesh B, r=1.56 is the mesh ratio from Mesh B to Mesh A

Table 5 - Air velocity (m s^{-1}), air temperature (°C), wall temperature (°C), moisture (%RH)

Parameter	Location	Device	No. Samples	Mean (Standard deviation)
Air Velocity	Inlet-A	Model 9545, TSI	50[a]	0.77 (0.04), 0.75 (0.04), 0.74 (0.04), 0.76 (0.03), 0.76 (0.04)
	Inlet-B	Model 9545, TSI	50[a]	0.78 (0.04), 0.76 (0.04), 0.74 (0.04), 0.74 (0.04), 0.76 (0.04)
	Middle Fan	Model 9545, TSI	50[c]	6.23 (0.18), 6.19 (0.16), 6.20 (0.15)
Air Temperature	Inlet-A	Model 9545, TSI	50[a,b]	20.0(0.01), 20.0 (0.01), 20.1 (0.01), 19.9 (0.02), 20.0 (0.01)
	Inlet-B	Model 9545, TSI	50[a,b]	20.3 (0.02), 20.2 (0.02), 20.1 (0.01), 20.3 (0.01), 20.2 (0.01)
	Atmosphere	Model 9545, TSI	50[a,b]	25.2(0.01)
Wall Temperature	Side Wall A	Model MT4 MAX, FLUKE	20[a]	25.1 (0.2), 25.2 (0.3), 25.0 (0.3) , 25.1 (0.1), 25.0 (0.3)
	Side Wall B	Model MT4 MAX, FLUKE	20[a]	25.3 (0.3), 25.3 (0.1), 25.0 (0.2) , 25.0 (0.3), 25.0 (0.1)
	Ceiling	Model MT4 MAX, FLUKE	20[a]	25.8 (0.1), 25.9 (0.2), 25.8 (0.2) , 25.7 (0.3), 25.9 (0.2)
	Floor	Model MT4 MAX, FLUKE	20[a]	23.0 (0.1), 22.9 (0.2), 22.9 (0.3) , 23.1 (0.1), 23.0 (0.3)
	Front Wall	Model MT4 MAX, FLUKE	20[a]	25.2 (0.3), 25.2 (0.3), 25.1 (0.3) , 25.2 (0.1), 25.0 (0.3)
	End Wall	Model MT4 MAX, FLUKE	20[a]	25.0 (0.2), 25.2 (0.3), 25.3 (0.3) , 25.3 (0.3), 25.2 (0.1)
Air Moisture	Inlet-A	Model 9545, TSI	50[a,b]	98.6 (0.2), 98.7 (0.2), 98.6 (0.4), 98.6 (0.2), 98.6 (0.2)
	Inlet-B	Model 9545, TSI	50[a,b]	98. 5 (0.2), 98.7 (0.3), 98.7 (0.3), 98.4 (0.2), 98.5 (0.1)
	Atmosphere	Model 9545, TSI	50[a,b]	62.2 (0.3), 62.5 (0.4), 62.3 (0.3), 62.3 (0.2), 62.5 (0.2)

[a] Parameters for each air inlet was measured at five points.
[b] Measurements were taken before and after the experiment.
[c] Air velocity was measured at 3 points at the end of the fan.

Table 6 - Boundary conditions at inlets and the outlet

Scenario	Inlet condition	Outlet condition
I	Pressure Inlet	Velocity Outlet
II	Velocity Inlet	Pressure Outlet
III	Pressure Inlet	Pressure Outlet
IV	Velocity Inlet	Airflow Rate Outlet

Table 7 - CFD Simulation settings and constants

Precision	3D Double Precision
Turbulence Mode	Realizable k-ε
Wall Treatment	Standard Wall Function
Pressure Velocity Coupling	Simple Algorithm
Discretization Scheme for Pressure	
Pressure	Second Order Upwind
Momentum	Second Order Upwind
Turbulent Kinetic Energy	Second Order Upwind
Turbulent Dissipation Rate	Second Order Upwind
Energy	Second Order Upwind
Air properties	
Density	1.225 kg m^{-3}
Cp	1006.43 J kg^{-1} K^{-1}
Thermal Conductivity	0.0242 W m^{-1} K^{-1}
Viscosity	$1.789 \cdot 10^{-5}$ kg m^{-1} s^{-1}
Atmospheric Pressure	101,325 Pa

Table 8 – Optimization of air inlets configurations

Case	Configuration	Remarks	Nondimensional total inlets area
I	Side-wall inlets	Experimental condition	1
II	Side-wall and Front- wall inlets	Side-wall air inlets are located at the front end of the house	1
III	Front-wall inlets	N/A	1
IV	Side-wall and Front- wall inlets	Side-wall air inlets are located at the middle of the house	1

Table 9 - Hosmer-Lemeshow test for different boundary conditions

Scenario	Chi-Square (χ^2)	df [a]	*p* value
I	8.762	8	0.363
II	10.126	8	0.256
III	7.555	8	0.478
IV	10.868	8	0.209

[a] df indicates the degree of freedom

Table 10 - Stepwise regression analysis results (p<0.05) for scenario III

Parameter	Coefficient	Standard Error
X	-1.570	0.912
Y	-3.404	0.309
Z	0.397	0.323
X^2	0.204	0.083
Z^2	-0.010	0.007
XY	0.215	0.364
XZ	-0.025	0.019
ZY	0.117	0.109
Constant	0.360	0.141

Table 11 - Differences between measured and CFD simulated air temperature: absolute differences (T_{CFD} - T_{EXP}) and relative differences E_r

Y=1.8 m				Y=0.8 m			
Sensor Number	**T_{CFD} - T_{EXP} (°C) [a]**	**T_{EXP} (°C)**	**E_r (%) [b]**	**Sensor Number**	**T_{CFD} - T_{EXP} (°C) [a]**	**T_{EXP} (°C)**	**E_r (%) [b]**
1	-0.18	20.3	0.92	16	0.81	24.0	3.39
2	0.11	21.4	0.54	17	2.16	24.3	8.90
3	-0.72	21.9	3.31	18	2.01	24.5	8.23
4	-0.35	21.8	1.59	19	1.15	24.3	4.76
5	-0.28	20.5	1.39	20	0.84	24.2	3.49
6	-0.98	22.8	4.34	21	0.81	22.4	3.63
7	0.94	23.0	4.09	22	1.87	22.2	8.45
8	0.05	23.6	0.23	23	1.00	22.5	4.48
9	0.65	23.2	2.83	24	1.48	22.3	6.65
10	-1.14	23.0	4.98	25	0.71	22.2	3.23
11	-1.07	25.1	4.27	26	0.17	20.8	0.85
12	0.09	26.1	0.36	27	0.28	21.4	1.32
13	-0.06	26.5	0.22	28	-0.66	21.7	3.04
14	0.25	26.0	0.94	29	0.66	21.2	3.14
15	-1.34	25.2	5.32	30	0.04	20.7	0.20

[a] T_{CFD} is CFD simulated air temperature, T_{EXP} is experimental measured air temperature

[b] $E_r = (|T_{CFD} - T_{EXP}| / T_{EXP}) \times 100$

Table 12 - Differences between measured and CFD simulated air velocity : absolute differences (V_{CFD} -V_{EXP}) and differences expressed as a percentage of bulk jet velocity (E_b)

Y=1.8 m				Y=0.8 m			
Sensor Number	**V_{CFD} - V_{EXP} (m s^{-1}) [a]**	**V_{EXP} (m s^{-1})**	**E_b (%) [b]**	**Sensor Number**	**V_{CFD} - V_{EXP} (m s^{-1}) [a]**	**V_{EXP} (m s^{-1})**	**E_b (%) [b]**
1	0.034	0.33	4.53	16	-0.014	0.4	1.86
2	-0.042	0.35	5.60	17	-0.072	0.4	9.60
3	-0.066	0.43	8.80	18	-0.031	0.46	4.80
4	-0.086	0.42	11.40	19	-0.075	0.4	10.00
5	0.063	0.27	8.40	20	-0.005	0.39	0.60
6	0.032	0.26	4.26	21	0.033	0.38	4.40
7	-0.045	0.42	6.00	22	0.027	0.44	3.60
8	-0.052	0.39	6.93	23	0.050	0.38	6.93
9	-0.029	0.37	3.86	24	-0.076	0.42	10.10
10	0.034	0.28	4.53	25	-0.024	0.39	3.20
11	0.032	0.28	4.26	26	0.079	0.31	10.50
12	-0.051	0.33	6.80	27	-0.033	0.39	4.40
13	0.041	0.28	5.46	28	-0.035	0.35	4.67
14	-0.025	0.33	3.33	29	0.049	0.42	6.53
15	0.036	0.29	4.80	30	-0.040	0.24	5.33

[a] V_{CFD} is CFD simulated air velocity, V_{EXP} is experimental measured air velocity

[b] $E_b = (|V_{CFD} - V_{EXP}| / V_0) \times 100$

Table 13 - Differences between measured and CFD simulated Relative Humidity(RH) : absolute differences (RH_{CFD} - RH_{EXP}) and relative differences E_r

Y=1.8 m				Y=0.8 m			
Sensor Number	**RH_{CFD} - RH_{EXP}** [a]	**RH_{EXP}**	**E_r (%)** [b]	**Sensor Number**	**RH_{CFD} - RH_{EXP}** [a]	**RH_{EXP}**	**E_r (%)** [b]
1	-0.6	96.2	0.62	16	-3.0	82.9	3.61
2	-1.8	92.0	1.95	17	-7.3	82.8	8.81
3	1.9	89.2	2.13	18	-7.8	83.4	9.35
4	-0.6	91.2	0.65	19	-7.7	83.0	9.27
5	-1.5	96.5	1.50	20	-3.0	82.5	3.63
6	4.6	83.8	5.48	21	-6.2	91.0	6.81
7	-3.5	85.6	4.10	22	-9.8	91.9	10.60
8	-0.5	82.7	0.61	23	-5.4	88.6	6.11
9	-1.1	83.3	1.32	24	-8.0	90.8	4.06
10	4.0	84.0	4.76	25	-5.6	91.1	6.14
11	7.0	74.3	9.42	26	-2.2	94.0	2.34
12	0.5	75.1	0.66	27	-5.6	94.7	5.91
13	1.9	72.7	2.61	28	-2.4	93.4	2.57
14	-0.1	75.5	0.13	29	-5.8	94.7	6.12
15	6.7	75.0	8.93	30	-3.4	96.2	3.55

[a] RH_{CFD} is CFD simulated relative humidity, RH_{EXP} is experimental measured relative humidity

[b] $E_r = (|RH_{CFD} - RH_{EXP}| / RH_{EXP}) \times 100$

Table 14 - Temperature at specific positions for different inlet configurations, unit: °C

Case		Sensor 11	Sensor 12	Sensor 13	Sensor 14	Sensor 15
I		24.7	26.2	26.8	26.2	24.4
II	Area ratio of side-wall inlets **:** front-wall inlets =2**:**1	24.6	25.9	26.6	26.0	24.2
II	Area ratio of side-wall inlets **:** front-wall inlets =1**:**1	24.3	25.8	26.2	25.7	24.1
III		24.2	25.6	26.0	25.7	24.1